ity under Different Shooting Parameters and Shooting Distances. Sensors Journal, IEEE , 2013,11,pp.99-102.
12. Xiaoming Li, Zhihan Lv, Baoyun Zhang, Ling Yin, Weixi Wang, Shengzhong Feng, Jinxing Hu. Traffic Management and Forecasting System Based on 3D GIS. 2015 15th IEEE/ACM International Symposium on Cluster, Cloud and Grid Computing (CCGrid). London,2015,pp.168-170.

Wavelet Sparse Representation based Beam-forming for Ultrasound Imaging: Theory and Simulation

Qiong Zhang[1,2] *, Minfen Shen[3], Bin Li[4] , Cheng Cheng[5]

[1] College of Engineering Shantou University, 515063 Shantou, Guangdong, China
[2] Guangdong Provincial Key Laboratory of Digital Signal and Image Processing Techniques, 515063 Shantou, Guangdong, China
[3] Shantou Polytechnic, 515078 Shantou, Guangdong, China
[4] Shantou Institute of Ultrasonic Instruments Co.,Ltd. 515041 Shantou, Guangdong,China
[5]Dept of Intelligent Multimedia Technology Research Center, Chongqing Institute of Green and Intelligent Technology, Chinese Academy of Sciences, 400714, Chongqing, China

Abstract
In this paper, a wavelet sparse representation based beamforming is proposed to improve the resolution and contrast of plane wave emission ultrasound imaging. First, the received signals are described as the convolution of the target scatterers with the point spread function of the system. And then, the wavelet sparse representation model is deduced according to the fact that the target scatterers can be sparse represented in wavelet domain. The proposed algorithm was tested with simulated ultrasound data in plane wave emission. And the results demonstrated that the resolution was clearly improved and contrast ratio gains of 9.8 dB, 4.3 dB and 3.7 dB were obtained compared to delay-and-sum beamformer, minimum variance beamformer and phase coherence factor, respectively.
Keywords: WAVELET SPARSE REPRESENTATION, ADAPTIVE BEAMFORMING, PLANE WAVE EMISSION, ULTRASOUND IMAGING, IMPROVE RESOLUTION AND CONTRAST

1. Introduction

The ultrasound device with plane wave (PW) emission, because of the broad transmit beams, has the potential to achieve high-frame-rate imaging which is a key factor in the applications of real-time 3D ultrasound imaging and ultrasound cardiac imaging [1][2]. In the receiving, the array signals are conventionally processed with delay-and-sum receiving

beamforming (DAS). Because of the non-adaptive of DAS, compared with the focused beam emission, the resolution and contrast are worse in the PW emission ultrasound imaging.

Recently, lots of beamformers have been proposed to improve the resolution and contrast of the broad transmit beam ultrasound imaging. Basically, the methods fall into two categories. One is element-space adaptive weighting, represented by minimum variance beamformer (MVBF) [3]-[7], which adaptively updates aperture weights by minimizing the power of the output subject to the constraint that the on-axis data must be preserved. However, the high degree of correlation among backscattering signals degrades the performance of the MVBF. The other is the beam-space adaptive weighting (BSW), represented by coherence factor (CF) [8]-[9] and phase coherence factor (PCF) [10][11], which weights the initial beamformed data using an index of focusing quality (IFQ) to preserve the on-axis data and cancel the off-axis ones. However, in these methods, the performance of IFQ decreases with the increase of the fire beam width.

Following the idea of BSW, a novel wavelet sparse representation based beamforming (WSRBF) is proposed. Wavelet sparse representation with an overcomplete basis is able to get an accurate IFQ in the correlated or even coherent backscattering signals in PW emission. Simulated results demonstrate that WSRBF is able to achieve high resolution and contrast ultrasound imaging in PW emission.

The abbreviations used in the paper were showed in Table I.

Table 1. The Abbreviations used in the Paper

Abbreviation	Full title
BSW	beam-space adaptive weighting
CF	coherent factor
CR	Contrast ratio index
DAS	delay-and-sum
FT	Fourier transform
IFQ	index of focusing quality
MVBF	minimum variance beamformer
PCF	phase coherent factor
PW	plane wave
ROI	region of interestion
WSRBF	wavelet sparse representation based beamforming

2. Basic Theory of Sparse Representation

Sparse representation has found applications in numerous domains [12], [13]. The problem of sparse signal representation is to find the signal s ($s \in C^L$) to satisfy

$$\min \|s\|_0^0 \text{ s.t. } x = As + n_{add} \tag{1}$$

where $x \in C^K$, $A \in C^{K \times L}$ is an overcomplete dictionary, i.e., K << L, n_{add} is an additional noise[14], [15]. However, (1) is a NP-hard (non-deterministic polynomial-time hard) problem in general. Recent results [16], [17] point out that if s is sufficiently sparse, they can be efficiently recovered by instead minimizing l_1-norm of l_0-norm. After replaced, the form of sparse representation is

$$\min\left[\|x - As\|_2^2 + \lambda \|s\|_1\right] \tag{2}$$

3. Proposed Method

3.1. Signal Model

In PW emission, assuming the incident wave at the point $\vec{\rho}_i$ in the ROI is denoted by $s_{\vec{\rho}_i}(t)$. The pulse-echo data received by the k-th element are denoted by $r_k(t)$. The scattering intensity at $\vec{\rho}_i$ is denoted by $f(\vec{\rho}_i)$. Without consideration of multiple scattering, the contribution of each point $\vec{\rho}_i \in$ ROI to $r_k(t)$ is $h(t) * \left[f(\vec{\rho}_i) \cdot s_{\vec{\rho}_i}(t - \tau_k(\vec{\rho}_i))\right]$ where $h(t)$ is the receiving impulse response of an element and $\tau_k(\vec{\rho}_i)$ is the time delay from $\vec{\rho}_i$ to the k-th element. Considering a discrete ROI with L grids, $r_k(t)$ can be expressed as

$$r_k(t) = \sum_{i=1}^{L} h(t) * \left[f(\vec{\rho}_i) \cdot s_{\vec{\rho}_i}(t - \tau_k(\vec{\rho}_i))\right] + n_k(t) \tag{3}$$

where $n_k(t)$ is the additive noise of the k-th element. In the frequency domain, (3) can be written as

$$(r_{wk}(w) = h_w(w) \cdot [\sum_{i=1}^{L} f(\vec{\rho}_i) \cdot s_{w\vec{\rho}_i}(w) \cdot \exp(-jw\tau_k(\vec{\rho}_i))] + n_{wk}(w) \tag{4}$$

where $r_{wk}(w)$, $h_w(w)$, $s_{w\vec{\rho}_i}(w)$, $n_{wk}(w)$ are the Fourier transform (FT) of $r_k(t)$, $h(t)$, $s_{\vec{\rho}_i}(t)$, $n_k(t)$ respectively. By defining $F = \left[f(\vec{\rho}_1), f(\vec{\rho}_1), \cdots, f(\vec{\rho}_L)\right]^T$, the FT of the received array signals is

$$R_w(w) = D(w) \cdot F + N(w) \tag{5}$$

where $\{\cdot\}^T$ denotes the nonconjugate transpose, $R_w(w) = \left[r_{w1}(w), r_{w2}(w), \cdots r_{wK}(w)\right]^T$, $D(w)$ is a K by L matrix with $[D(w)_k]_i = h_w(w) s_{w\vec{\rho}_i}(w) \cdot \exp[-jw\tau_k(\vec{\rho}_i)]$, $N(w) = \left[n_{w1}(w), n_{w2}(w), \cdots n_{wK}(w)\right]^T$.

3.2. Wavelet Sparse Representation based Beamforming

Because K << L, (5) is ill-posed. As F is the scattering intensities of the imaged medium, according to the theory of multi-scale signal sparse representation

[18], there exists a wavelet basis Φ and the sparse vector C, such that $F = \Phi C$. Therefore (5) can be represented as

$$R_w(w) = D(w)\cdot(\Phi C) + N(w) = \left[D(w)\cdot\Phi\right]\cdot C + N(w)$$
$$\text{s.t. } C \text{ sparse} \qquad (6)$$

As the purpose is to get the *IFQ*, (6) can be solved at the fire center frequency f_0 to reduce computation.

$$\min\left[\left\|D(2\pi f_0)\cdot\Phi\cdot C - R_w(2\pi f_0)\right\|_2^2 + \lambda\|C\|_1\right] \qquad (7)$$

Let $D_\Phi(2\pi f_0) = D(2\pi f_0)\cdot\Phi$, then (7) can be written as

$$\min\left[\left\|D_\Phi(2\pi f_0)\cdot C - R_w(2\pi f_0)\right\|_2^2 + \lambda\|C\|_1\right] \qquad (8)$$

After solving (8), the *IFQ* can be calculated as $IFQ = \Phi C$. The processing diagram of WSRBF is shown in Fig.1. After the received pulse echo data are digitized by ADCs, parallel DAS is performed to form the initial image. The final image are then obtained by weighting the initial image with *IFQ*.

4. Analysis of Inclination

A phantom with a circular cyst and four point targets in a speckle pattern was simulated to compare the resolution and contrast of the WSRBF with that of DAS, PCF, and MVBF. The circular cyst has a radius of 3 mm and center at (x, z) = (0, 50) mm. And the four point targets are located at (x, z) = {(0, 60), (-3.4, 65), (0, 65), (0.5, 65)} mm. The Field II [19] was used to generate channel data in PW emission with a 5 MHz, 80% bandwidth, 96-element, half-wavelength spacing linear array transducer. The db4 wavelet was used to construct the dictionary. In the WSRBF, the ROI was discretized every 0.15mm axially and every 0.1mm laterally and the regularization parameter in (8) was set 0.6 by experience. For the MVBF, we used subarray length $V = K/2$ (K is the number of elements) and the diagonal loading parameter $\Delta = 1/(100\,V)$ to ensure a well-conditioned covariance matrix. The contrast ratio index (CR), defined as the ratio of the mean value of the background to that of the cyst region [20], is used to evaluate the enhancement of the contrast.

Fig.2 shows the beamformed responses of the phantom via the DAS, MVBF, PCF and WSRBF and the corresponding lateral variation at depth z = 60 mm is shown in Fig. 3. It is shown that all the point targets can be resolved clearly in Fig. 2(d) and the mainlobe width of the WSRBF is about 16.6% that of DAS, 20.1% that of MVBF and 30.7% that of PCF in the speckle pattern. And CR gains of 9.8 dB, 4.3 dB and 3.7 dB were obtained compared to DAS, MVBF and PCF, respectively. Therefore, the WSRBF presents the narrowest mainlobe, the lowest sidelobe level and the highest contrast among the four methods.

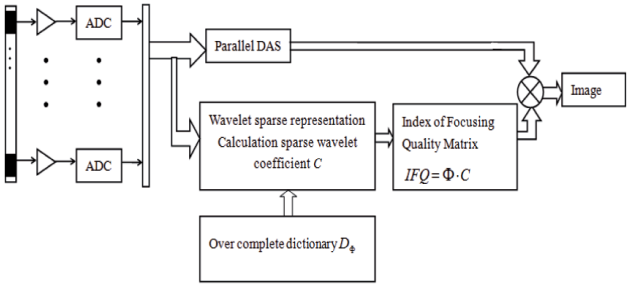

Figure 1. Block Diagram of Signal Processing of the Proposed WSRBF. DFT is the Discrete Fourier Transform. And $D_\Phi = D\cdot\Phi$ is the Wavelet Overcomplete Dictionary.

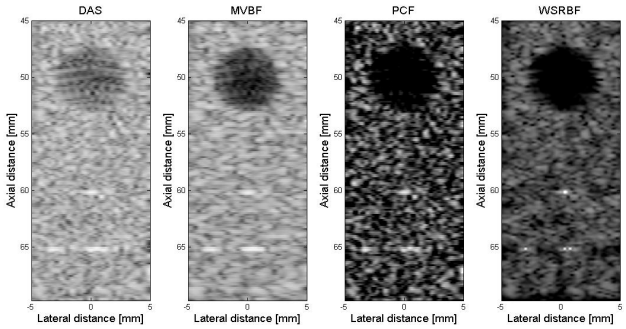

(a) (b) (c) (d)

Figure 2. Beamformed responses of the circular cyst and four point targets in a speckle pattern with a 5-MHz, 80% bandwidth, 96-element, half-wavelength spacing linear array in the PW emission. The circular cyst has a radius of 3 mm and center at (x, z) = (0, 50) mm. And the four point targets are located at (x, z) = {(0, 60), (-3.4, 65), (0, 65), (0.5, 65)} mm. (a) DAS, (b) MVBF, (c) PCF and (d) WSRBF. All images are shown with a dynamic range of 60 dB.

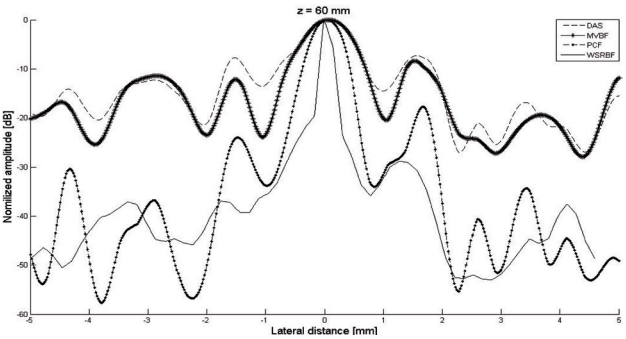

Figure 3. Lateral variation at z = 60 mm of the beamformed responses shown in Fig. 2(a)-(d). The point target is located at (x, z) = (0, 60) mm.

Conclusions

A novel receiving beamforming based on the wavelet sparse representation, named WSRBF, has

been proposed to improve the resolution and contrast of ultrasound imaging with the PW emission. Simulated results demonstrated the effectiveness of the proposed method. The excellent performance of the WSRBF could be explained by the IFQ calculated by the wavelet sparse representation which translates into narrowed mainlobe, reduced sidelobes and enhanced contrast when compared to DAS, MVBF and PCF in PW emission.

Acknowledgment

This work is supported by Specific Discipline Construction Fund of Guangdong (No.cgzhzd1105) and Science and Technology Planning Project of Guangdong Province, National Natural Science Foundation of China (No. 61302049), Natural Science Foundation of Guangdong (No.S20130400117 86) and Open Fund of Guangdong Provincial Key Laboratory of Digital Signal and Image Processing Techniques(2014GDDSIPL-05).

References

1. S. Salles, H. Liebgott, O. Basset, ect, Experimental evaluation of spectral-based quantitative ultrasound imaging using plane wave compounding, IEEE Trans. Ultrasonics, Ferroelectrics and Frequency Control, 2014, 61, pp.1824-1834.
2. Jesper Udesen, Fredrik Gran and Jensen, J.A., High frame-rate blood vector velocity imaging using plane waves: simulations and preliminary experiments, IEEE trans. Ultrasonics, Ferroelectrics, and Frequency Control, 2008,55, pp. 1729-1743.
3. S. L. Wang, and P.-C. Li MVDR-based coherence weighting for high-frame-rate adaptive imaging, IEEE trans. Ultrasonics, Ferroelectrics, and Frequency Control, 2009, 56, pp. 2097-2110.
4. J. F. Synnevag, C. I. C. Nilsen, and S. Holm, Speckle statistics in adaptive beamforming, Proceedings of the IEEE Symposium on Ultrasonics, 2007, 12,pp.1545-1548.
5. J. F. Synnevag, A. Austeng and S. Holm, Benefits of minimum-variance beamforming in medical ultrasound imaging, IEEE trans. Ultrasonics, Ferroelectrics, and Frequency Control, 2009,56, pp. 1868-1879.
6. I.K. Holfort, F. Gran and J.A. Jensen, Broadband minimum variance beamforming for ultrasound imaging, IEEE trans. Ultrasonics, Ferroelectrics, and Frequency Control, 2009,56, pp. 314–325.
7. J. F. Synnevag, A. Austeng and S. Holm, Adaptive beamforming applied to medical ultrasound imaging, IEEE trans. Ultrasonics, Ferroelectrics, and Frequency Control, 2007,54, pp.1606-1613.
8. P.-C. Li and M.-L. Li, Adaptive imaging using the generalized coherence factor, IEEE trans. Ultrasonics, Ferroelectrics, and Frequency Control, 2003,15, pp. 128-141.
9. Chi Hyung Seo and Jesse T. Yen, Sidelobe suppression in ultrasound imaging using dual apodization with cross-correlation, IEEE trans. Ultrasonics, Ferroelectrics, and Frequency Control, 2008,55, pp. 2198-2210.
10. Jorge Camacho, Montserrat Parrilla and Carlos Fritsch, Phase coherence imaging, IEEE trans. Ultrasonics, Ferroelectrics, and Frequency Control, 2009,56, pp. 958-974.
11. Hideyuki Hasegawa and Hiroshi Kanai, Effect of subaperture beamforming on phase coherence imaging, IEEE Trans. Ultrasonics, Ferroelectrics and Frequency Control, 2014,61, pp. 1779-1790.
12. M. Çetin and W. C. Karl, Feature-enhanced synthetic aperture radar image formation based on nonquadratic regularization, IEEE Trans. Image Process., 2001,10, pp. 623–631.
13. Shenghua Gao, Ivor WH Tsang and Liangtien Chia,Sparse representation with kernels, IEEE Trans. Image Processing, 2013,22, pp.423-434.
14. J. J. Fuchs, Detection and estimation of superimposed signals, IEEE Int. Conf. Acoust., Speech, Signal Process., 1998, 3,pp. 1649-1652.
15. B. D. Rao and K. Kreutz-Delgado, Basis selection in the presense of noise, Thirty-Second Asilomar Conf. Signals, Syst., Comput., 1998, 1,pp. 752-756.
16. D.Donoho, For most large underdetermined systems of linear equations the minimal 1-norm solution is also the sparsest solution, Commun. Pur. Appl. Math.,2006,59, pp.797-829.
17. S. S. Chen, D. L. Donoho, M. A. Saunders, Atomic decomposition by basis pursuit, SIAM Journal on Scientific Computing, 1998, 20, pp. 33–61.
18. Angela Kunoth, Adaptive wavelets for sparse representations of scattered data, Studies in Computational Mathematics, 2006,12, pp. 85-108.

19. J. A. Jensen, Field: A program for simulating ultrasound systems, Med. Biol. Eng. Comp., 10th Nordic-Baltic Conference on Biomedical Imaging, 1996,4, pp. 351-353.
20. O'Donnell and S. W. Flax, Phase-aberration correction using signals from point reflectors and diffuse scatterers: measurements," IEEE trans. Ultrasonics, Ferroelectrics, and Frequency Control, 1998,35,pp.768-774.

Brain CT Image Classification Based on Improving Harmony Search Algorithm Optimize LSSVM

Xu li[1], Bai jinniu[2], Li leimin[3]

1. Inner Mongolia University of Science and Technology Department of Computer Science and Technology, Baotou Medical College, Inner Mongolia Baotou, 014060 China
2. Inner Mongolia University of Science and Technology Department of Computer Science and Technology, Baotou Medical College, Inner Mongolia Baotou, 014060 China
3. School of National Defence Science and Technology, Southwest University of Science and Technology , Sichuan Mianyang, 621010 China

Abstract
In order to enhance the accuracy of brain CT image classification, this article proposes a brain CT image classification of improving harmony search algorithm to optimize LSSVM(HIS-LSSVM) aiming at the optimization problems of parameters of least squares support vector machine (LSSVM)in the classifier. This article first takes LSSVM parameters as a combination of tones from different musical instruments and then finds the optimal parameters through "tone tuning" of harmony search algorithm. It also introduces optimal position adjustment policy of particle swarm optimization to strengthen the algorithm's capability to jump out of local minimum. At last, this article establishes brain CT image classification model according to optimal parameters and implements simulation test to the performance of the model. It is shown from the simulation results that comparing with the contrast model, HIS-LSSVM not only enhances the accuracy of brain CT image classification, but also increases classification speed. It is more suitable for the real-time classification requirements of brain CT image.
Keywords: BRAIN CT IMAGE CLASSIFICATION, LEAST SQUARES SUPPORT VECTOR MACHINE, HARMONY SEARCH ALGORITHM, PARTICLE SWARM OPTIMIZATION

1. Introduction

In recent years, radiodiagnosis equipment is continuously renewed and perfected. Hospitals have collected a large amount of brain CT image data of patients. It becomes more and more important to dig information from these image data which can help doctors diagnose patients. The image classification is an important research content for brain CT image